Published in final edited form as:
Acta Biomater. 2019 September 01; 95: 297–306. doi:10.1016/j.actbio.2019.06.030.

Bi-layered micro-fibre reinforced hydrogels for articular cartilage regeneration☆

Miguel Castilho[a,b,c,*], **Vivian Mouser**[b], **Mike Chen**[d], **Jos Malda**[a,c,e], **Keita Ito**[a,b,c,*]

[a] Department of Orthopaedics, University Medical Center Utrecht, Utrecht, The Netherlands [b]Orthopaedic Biomechanics, Department of Biomedical Engineering, Eindhoven University of Technology, Eindhoven, The Netherlands [c] Regenerative Medicine Utrecht, Utrecht, The Netherlands [d]School of Mathematical Sciences, The University of Adelaide, Adelaide, SA, Australia [e] Department of Functional Materials in Medicine and Dentistry, University of Würzburg, Würzburg, Germany

Abstract

Articular cartilage has limited capacity for regeneration and when damaged cannot be repaired with currently available metallic or synthetic implants. We aim to bioengineer a microfibre-reinforced hydrogel that can capture the zonal depth-dependent mechanical properties of native cartilage, and simultaneously support neo-cartilage formation. With this goal, a sophisticated bi-layered microfibre architecture, combining a densely distributed crossed fibre mat (superficial tangential zone, STZ) and a uniform box structure (middle and deep zone, MDZ), was successfully manufactured via melt electrospinning and combined with a gelatin-methacrylamide hydrogel. The inclusion of a thin STZ layer greatly increased the composite construct's peak modulus under both incongruent (3.2-fold) and congruent (2.1-fold) loading, as compared to hydrogels reinforced with only a uniform MDZ structure. Notably, the stress relaxation response of the bi-layered composite construct was comparable to the tested native cartilage tissue. Furthermore, similar production of sulphated glycosaminoglycans and collagen II was observed for the novel composite constructs cultured under mechanical conditioning w/o TGF-ß1 supplementation and in static conditions w/TGF-ß1 supplementation, which confirmed the capability of the novel composite construct to support neo-cartilage formation upon mechanical stimulation. To conclude, these results are an important step towards the design and manufacture of biomechanically competent implants for cartilage regeneration.

Keywords

Cartilage regeneration; Fibre-reinforced hydrogels; Superficial tangential zone; Melt electrowriting; Osteoarthritis

*Corresponding authors at: Department of Orthopaedics, University Medical Center Utrecht, Utrecht, The Netherlands and Department of Biomedical Engineering, Eindhoven University of Technology, Eindhoven, The Netherlands. M.DiasCastilho@umcutrecht.nl (M. Castilho), K.Ito@tue.nl (K. Ito).
☆Part of the Cell and Tissue Biofabrication Special Issue, edited by Professors Guohao Dai and Kaiming Ye.

Europe PMC Funders Author Manuscripts

Europe PMC Funders Author Manuscripts

1 Introduction

The inability to treat articular cartilage damage has driven intensive efforts in orthopedic research over the last few decades. Currently, the standard clinical treatment for joint degeneration is a total joint replacement using metallic prostheses, which lack biologically adaptive properties and thus have a limited life span [1]. A proposed alternative is to replace damaged cartilage with a bioengineered regenerative implant. Ideally, such an implant would promote new tissue formation, while simultaneously mimicking the biomechanical properties of cartilage. This entails the use of degradable scaffold materials as carriers and/or delivery vehicles for mature (or progenitor) and autologous (or allogeneic) chondrocytes capable of cartilage formation [2–4]. Although promising, the bioengineered constructs typically exhibit inferior strength and stiffness compared to native cartilage and feature isotropic cell distribution, as opposed to the zonal cell distribution and composition seen in healthy cartilage.

Native cartilage is comprised of four main components: chondrocytes, proteoglycan macromolecules (PGs), collagen type II fibrils and water. These are distributed heterogeneously in three distinct zones: the superficial tangential (STZ), middle (MD) and deep zone (DZ) [5]. From a functional perspective the cartilage is often simplified into two principal zones: the STZ (representing 10–20% of cartilage thickness) [6] which support tensile loads, distributes compressive loads and ensure frictional properties; and the middle and deep zone (80–90% of cartilage thickness) which together are responsible for the support of compressive loads by ensuring a high osmotic pressure and low permeability. In particular, it has been shown that the tightly packed and tangential oriented collagen fibres present in the STZ zone are key to ensuring the normal mechanical function of cartilage. The fibres act to distribute axial loads laterally through inducing tensile stress parallel to the surface and thus recruiting a larger volume of underlying tissue to support the load than just that immediately below the contact surface [7].

A few studies have attempted to fabricate multi-layered scaffolds to capture the complexity of native cartilage. Predominantly, the manufacturing approaches have relied on solution electrospinning of fibre materials [8], gas foaming or particulate template of porous polymeric structures [9], densification of collagen matrices [10], or extrusion-based 3D printing of cell laden gels [11]. Each manufacturing technique offered its own advantages, however none can (yet) fully replicate the structural organization and functional properties of native cartilage. More recently, we reported on the reinforcement of soft cell-laden hydrogels with organized micro-fibre scaffold obtained by direct melt electrospinning (MEW) [12–14]. Although abundant matrix formation was observed in these novel composite constructs, they were still not able to ensure adequate mechanical integrity after implantation nor guide zonal tissue formation. We hypothesize that this may have been due to a lack of a superficial tangential zone (STZ) -like structure. In fact, clinical studies have revealed that the disruption of the superficial zone collagen fibres during the early stages of articular cartilage degeneration appears to be the main mechanism for cartilage softening and its subsequent progressive mechanical deterioration [15,16]. Therefore, the incorporation of a viable superficial tangential zone into tissue engineered constructs appears fundamental for proper mechanical function.

We aim to develop and characterize a bi-layered fibre reinforced cell-laden hydrogel construct that captures the functional properties of both the STZ and MDZ zones of native cartilage. Specifically, we have designed and 3D printed different microfibre scaffold architectures to reinforce a gelatin–methacrylamide (GelMA) hydrogel system, i.e. a densely distributed crossed fibre mat (STZ); fibres printed in a uniform box structure (MDZ); and a combination with a construct height consisting of a upper layer of 10% STZ and a lower layer of 90% MDZ (STMDZ). The time-dependent mechanical response of these composite constructs was characterized under unconfined compression and macro-indentation to mimic congruent and incongruent joint loading. Osteochondral cores of porcine knee joints with and without a superficial layer were also characterized under the same loading conditions to elucidate the biomimetic nature of the engineered constructs. A final aim was to investigate whether the novel STMDZ composite constructs could support and direct chondrogenesis under dynamic mechanical conditioning.

2 Experimental section

2.1 Fibre scaffolds fabrication via melt electrowriting

A custom-built MEW printer was used, as described previously [13]. Briefly, GMP-PCL (PURASORB PC 12, Corbion Inc., Netherlands) was melted in a 3 cc glass syringe at 85 °C and extruded through a 23 G spinneret connected to a high voltage source (LNC 10000-5 pos, Heinzinger Electronic GmbH, Germany). Electrified polymer jets were collected in a layer-by-layer fashion onto a grounded computer-controlled collector plate. To allow homogeneous collection of fibres, the key MEW parameters, acceleration voltage (U), air pressure (P), and collector velocity (V) were set at 5-6.5 kV, 2 bar and 5-6 mm/s, respectively. Three scaffold architectures were designed using a machine specific coding language (PMX-2EX-SA, ARCUS Technology- Inc., USA): a STZ comprising fibres laid-down at 0-45-90-135° alternately; an MDZ, comprising a cross-shaped 0-90° lay-down pattern; and a combination with construct height of 10% STZ and 90% MDZ (STMDZ). Fibre diameter and scaffold microstructure was imaged by scanning electron microscope (Phenom Pro, Phenom-World, The Netherlands) at an acceleration voltage of 5-10 kV and images were subsequently analyzed with ImageJ (National Instruments, USA). Scaffolds porosity was measured gravimetrically.

2.2 Cell-free fibre reinforced hydrogels preparation

GelMA with an 80% degree of methacrylation was synthesized by reacting gelatin from porcine skin (Sigma Aldrich, gelatine Type A, The Netherlands) with methacrylic anhydride (Sigma Aldrich, The Netherlands) following a procedure described elsewhere [17,18]. Fibre reinforced cylindrical hydrogels with 1 mm height and diameters of 5 or 8 mm were prepared in Polytetrafluoroethylene molds (PTFE; Teflon®). Fibre networks were first cut to the proper size from printed meshes (6×6 cm), and placed into the molds where 10% (w/v) gelMA together with crosslinker solution (Irgacure at 0.1% w/v in PBS) was cast. Samples were then UV crosslinked by exposure to 365 nm UV light for 15 min (UV-Handleuchte lamp A. Germany. Intensity 2.6 mW/cm^2). After preparation, high-resolution micro-CT (μCT) analysis was performed using a micro-CT scanner (μCT 80, Scanco Medical AG, Switzerland) at a voltage of 70 kVp, an intensity of 114 μA and an integration time of 300

ms (Gauss filter applied, sigma = 1, support = 0.8 voxel). A water-based contrast agent solution (Ioversol, Optiray 300 TM) was used for staining the GelMA hydrogel during μCT analysis.

2.3 Osteochondral plugs preparation

Twenty osteochondral plugs were harvested from 4 porcine knee joints (tibial plateau) of 2-4 year-old animals obtained from a local slaughterhouse under local regulations. Cores with a diameter of 5 and 8 mm were extracted perpendicular to the articular surface using a custom-made cutting tool. After harvesting, the subchondral bone thickness was trimmed to approximately 5 mm and plugs were stored at -20 °C until further use. On each day of mechanical testing samples were thawed in room temperature running water and the thickness of the articular cartilage was measured microscopically (Olympus SZ61). A microtome was used to remove the surface layer (approximately 15-20% of the cartilage thickness) from half of the plugs and then final thickness was re-measured. In total 10 plugs of full-thickness cartilage (Intact) and of cartilage deprived of the surface layer (Less STZ) were prepared.

2.4 Mechanical testing

The mechanical properties of both the engineered constructs and the native cartilage of the osteochondral plugs were assessed by unconfined compression (UC), with a flat-ended platen with a 10 mm diameter, and macro-indentation (IND), with a rigid cylindrical indenter of 2 mm radius with a hemi-spherical tip of 1 mm radius. Samples for UC were 5 mm diameter and 1 mm thick, while for INC were 8 mm diameter and 1 mm thick. Tests were performed on a universal testing machine (Zwick Z010, Germany) equipped with a 20 N load cell. Prior to testing samples were fixed to the bottom of a custom-made polycarbonate container using a cyanoacrylate-based adhesive. The test container was then filled with PBS and all mechanical tests were performed with samples fully immersed in PBS to approximate physiological conditions. Stress relaxation testing was performed on both UC and IND experiments. For UC testing a pre-load of 0.01 N was first applied to test samples and then strained to 20% at a rate of 10 μm/s, followed by a relaxation period of 900 s. For IND testing a pre-load of 0.005 N was first applied to ensure initial contact between the test samples and the hemi-spherical indenter and then strained to 20% at rate of 10 μm/s, followed by a relaxation period of 900 s. At least 5 samples were analyzed per group, *i.e.* hydrogel alone; STZ, MDZ, STMDZ reinforced hydrogels and Intact and STZ-removed native cartilage. The STZ - MDZ adhesion strength was investigated by a qualitative peel test, which involved manually detaching the STZ from the MDZ layer.

2.5 Mechanical data analysis

Stress-strain curves were calculated from the applied force and displacement data from the UC and IND loading experiments. Here, stress is defined as the applied force divided by the specimen's unloaded cross-sectional area. For the IND experiments the loaded area was approximated as the transverse cross-sectional area of a flat ended cylindrical indenter (Ø = 4 mm), $\approx 12.6 mm^2$, and is assumed to be constant throughout the loading period. Although in reality this area will vary as the indenter is lowered, this simplifying assumption is adequate here since the main point of interest is to compare the response of differently

engineered constructs to the same loading strategy. The actual contact area was not determined. Peak and equilibrium stresses were calculated from each stress relaxation curve at peak or equilibrium, respectively. Strain was defined as the ratio between the original sample thickness and the displacement of either the flat ended platen (UC) or the indenter (INC). For each relaxation test we have calculated the apparent peak modulus during the ramp phase from the slope of the stress-strain curve near the maximum value of stress. We also report on the apparent equilibrium modulus, which is calculated by dividing the stress at the final recorded time by the corresponding strain. To quantify the relaxation response a piecewise exponential function was fitted to the obtained stress-time curves following Thambyah and Broom method [19]. The fitted curves consist of three segments corresponding to an initial loading phase, and a fast and a slow relaxation phase. The formulae for the exponential curves for the fast and slow relaxation phases used are as follows,

$$\sigma(t) = \begin{cases} Ae^{-t/\tau} + B, & t < 100 \\ \cdot & \\ Ae^{-t/\tau} + B, & t \geq 100 \end{cases} \quad (1)$$

where the coefficients A and B are statistical parameters quantifying the shape of the relaxation curves and s is a time constant that determines the rate of stress relaxation. The fitting procedure minimizes the root mean square error between these curves and the measured stress, subject to the constraints that the fitted curves match the peak and equilibrium stress and that the two curves match at t = 100 s. The switchover point of 100 s was determined by performing a further fit on the DZ data, where this switching point was allowed to vary; a value of approximately 100 s minimised the mean square error and so was used throughout. This slightly simpler model, with a fixed switchover point, has the advantage that it permits a straightforward comparison between the sample groups. We have verified that for a subset of data allowing the crossover point to float does not alter the overall conclusions. Note that the parameters that result from this fitting procedure together with the determined apparent peak and equilibrium moduli, only describe the observed behavior rather than giving information about the underlying material properties of the engineered constructs or native cartilage. These moduli were determined solely to facilitate comparison between tested samples under the same loading conditions.

2.6 Cell-laden fibre reinforced hydrogels preparation

Chondrocytes were harvested from healthy cartilage of equine metacarpophalangeal joints (3 donors, 4-8 years old), following a standard lab protocol described elsewhere [20]. After harvesting, and expanding the cells, chondrocytes (passage 1) were suspended in 10% (w/v) gelMA at a concentration of $20 * 10^6$ chondrocytes/ml, and subsequently injected into the printed fibre networks housed in sterile PTFE molds. Fibre scaffolds were sterilized by ethanol (70% ethanol, 5 min soaking) and then UV light exposure (20 min on both sides). Composites constructs with 8 mm in diameter and 1 mm in height were then UV-crosslinked for 15 min as described in Section 2.2.

2.7 In vitro culture

Cell-laden constructs were divided into three groups; 1) samples were cultured in basal medium (96 ml of Dulbecco's modified Eagle medium, 31966 Gibco, Netherlands; 1 ml ITS + premix, 35432 Gibco; 1 ml ascorbic acid-2-phosphate; 1 ml of penicillin and streptomycin; 4 ll of dexamethasone); 2) samples were cultured in basal medium supplemented with TGF-ß1 (10 ng/mL) and 3) samples were cultured in base medium with mechanical conditioning. All three groups were cultured for 28 days at 37 °C, 5% CO_2 and 95% humidity. The medium was refreshed twice a week. Only cell laden gels reinforced with MDZ and STMDZ architectures were analyzed, however pilot experiments were also performed on non-reinforced cell laden hydrogels. For condition 3, constructs were mechanically conditioned under dynamic compression using a custom-built bioreactor system (as schematized in Fig. 4C). The core system consisted of eight stimulation units housed in a water bath that was placed in a dynamic testing device (MTS Acumen, USA). All the stimulation units were loaded simultaneously by using individual spring-based pistons with a hemi-spherical rigid indenter of 4 mm radius. A dynamic load was applied from 0 to ~15%/20% amplitude strain in a sinusoidal waveform at a frequency of 1 Hz. After each loading session, the samples remained in culture medium under standard conditions (37 °C in 5% CO_2 and 95% humidity). At least 4 samples of each group were tested.

2.8 Biochemical assays and histological examination

After 1 and 28 days of in *vitro* culture under the different conditions, the samples were divided in two halves, one for biochemical assessment and the other for histological examination. For biochemical assessment each sample was weighed, freeze dried and digested in papain digest buffer (0.2 M NaH_2PO_4, plus 0.01 M EDTA*$2H_2O$ in milliQ, pH = 6.0) supplemented with 250 µl/ml papain solution (16-40 units/mg protein, P3125, Sigma Aldrich) and 0.01 M cysteine (C9768, Sigma Aldrich) overnight at 60 °C. Digested samples were assayed for DNA content using a Quant-iT, Picogreen kit (Thermo Fischer Scientific) and for GAGs using a dimethylmethylene blue assay (DMMB, Sigma Aldrich). For histology, each sample was fixed overnight in formalin, dehydrated through graded ethanol series and embedded in paraffin. Fixed samples were then cleared in xylene, sectioned at a thickness of 5 µm, and stained with hematoxylin (cell nuclei), Safranin-O (proteoglycans), and Fast green (collagen), as previously described [20]. In addition, immunohistochemistry was used to visualize collagen type II [20]. Cell viability was determined at day 1 using a LIVE/DEAD assay (2 µM Calcein AM, 2 µM Ethidium homodimer, Thermo Fisher Scientific). Of each sample, 3 images were made at different locations and cell viability was quantified by manually counting the cells.

2.9 Statistical analysis

A one-way ANOVA with Tukey's post hoc test was used to compare the means of the different groups. Test differences were considered significant at a probability error (p) of $p < 0.05$, or as indicated. Normality and homogeneity were checked with Shapiro-Wilks and Levene's tests, using Excel and/or IBM SPSS 23 software.

3 Results

3.1 Fabrication of bilyared fibre reinforced hydrogels

Fibre scaffolds with a well-defined bi-layered organization were successfully manufactured by melt electrowriting (Fig. 1 and supplementary information, Movie S1). SEM images show the tangen-tially oriented and angle-plied fibres in the STZ (Fig. 1B), and the consistently stacked fibres in a box-like microstructure in the MDZ (Fig. 1C). All scaffolds exhibited an accurate fibre placement without significant fibre distortion or deviation in fibre diameters (≈20 μm) as shown in Fig. 1D and E. By first printing the STZ architecture and then the MDZ architecture onto it, it was possible to manufacture the entire construct in a single print and ensure sufficient adhesion and integration between the two architectures. All constructs yielded final thicknesses of ≈1.0 mm and had an open and fully interconnected porosity of 70 ± 4% and 97 ± 4% in the STZ and MDZ layers, respectively. Following printing, the fibre scaffolds were successfully combined with a GelMA hydrogel (Fig. 1F). Results of μCT analysis confirmed a uniform distribution of the hydrogel inside both STZ and MDZ regions (Fig. S1).

3.2 Role of superficial layer on reinforced constructs mechanical behavior

A significant improvement on the construct's modulus was observed when gelMA hydrogels were reinforced with the bilayered fibre architecture. The peak modulus of the STMDZ constructs increased by ≈2.1-fold under congruent loading and notably by ≈3.2-fold under incongruent loading, when compared to the MDZ reinforcement (Fig. 2). This mechanical reinforcement was remarkably larger when compared to the unreinforced gels with an ≈12-fold increase under congruent loading, and close to ≈20-fold increase under in-congruent loading. Interestingly, the MDZ composites were stiffer than STZ constructs under congruent loading (225.7 ± 14.4 vs. 173.3 ±28.9 kPa) but were not significantly different under in-congruent loading (35.5 ± 10.2 vs. 30.2 ± 3.9 kPa). Also, the ratio between the peak and equilibrium stress was observed to be significantly higher for the STMDZ reinforced gels when compared with the unreinforced gels or MDZ, mostly under congruent loading conditions. The same qualitative effect is shown in supplementary information (Table S1) with the results reported in terms of the peak and equilibrium moduli (in kPa), and the ratio between the two moduli.

The STZ layer also showed a significant effect on the relaxation response of the reinforced gels. To quantify this effect, exponential functions were fitted to the fast and slow decay regions of the stress relaxation curves. A typical stress-time curve is shown in Fig. 2B against a fitted exponential curve with a RMSE value less than 0.05. As summarized in Fig. 2C, for unconfined compression the initial stress relaxation response is similar for all four constructs, but the subsequent slow relaxation to the equilibrium stress is steeper for the STMDZ construct. This is in contrast to the results for in-congruent loading, as shown in Fig. 2D. For this loading condition, the MDZ and STMDZ constructs display rapid initial relaxation compared to the GelMA and STZ constructs, with all four constructs displaying similar relaxation rates to their respective equilibrium stress values.

Europe PMC Funders Author Manuscripts

3.3 Role of superficial layer on native cartilage mechanical behavior

Removal of the top cartilage region was first evaluated by histological analysis of GAG distribution. Intact cartilage demonstrated a consistent gradient of GAGs across the sample thickness, where GAG content was lower in the superficial zone and higher in the middle and deep zone (Fig. 3A). Instead, STZ removed samples had a higher and even distribution of GAGs across the sample thickness, which confirmed effective removal of the top cartilage region. Overall, the average cartilage thickness of osteochondral cores was 2.2 ± 0.2 mm for intact cartilage (Intact) and 1.7 ± 0.3 mm after removal of the STZ-region (w/o STZ); representing approximately 20% of cartilage full thickness removed. Moreover, osteochondral cores were used for mechanical characterization instead of isolated cartilage, as we observed the bone attachment facilitated superficial layer removal without affecting the remaining collagen network significantly, and also allowed an easy fixation during mechanical testing.

Under congruent loading the removal of STZ resulted in a small but significant increase, ≈1.2-fold, in cartilage peak modulus (Fig. 3B), while no significant differences were observed under in-congruent type loading (Fig. 3C). In contrast, the ratio of peak to equilibrium stress of STZ-removed samples significantly decreased under both congruent and in-congruent loading being ≈2.1-fold and ≈1.7-fold lower, respectively. In regards to the relaxation rates, significant differences between intact and STZ-removed cartilage were only observed under congruent loading conditions, where the STZ-removed samples displayed a significant slower initial ($p = 0.125$) and late stress relaxation decay ($p = 0.247$). A comparable analysis in term of peak and equilibrium moduli, and the ratio between these quantities, is given in supplementary information (Table S1) and shows similar effects to those shown in Fig. 3.

3.4 Bi-layered fibre scaffolds support neo-cartilage formation under dynamic loading

Cell viability was assessed at day 1 showing over 80% of viability of chondrocytes in both MDZ and STMDZ scaffolds cultured under static or dynamic loading conditions (Fig. 4A). Chondrocytes were uniformly distributed over both scaffold architectures. Specifically, cells were observed to penetrate the STZ region despite its high fibre density and reduced porosity.

As for the deposition of neo-cartilage extracellular matrix (ECM) components, all sample groups were observed to maintain their chondrogenic phenotype and synthesized GAGs after 28 days of *in vitro* culture (Fig. 4B). No significant differences in GAG production were observed between the gelMA samples reinforced with MDZ and STMDZ structures for any of the culture conditions. Interestingly, the addition of TGF-ß1 in static culture or using mechanical conditioning without TGF-ß1 supplementation showed a similar increase in GAG production when compared to static culture in pure basic medium (≈3.4-fold for TGF-ß1 and 3.0-fold for mechanical stimulation w/o TGF-ß1). Histological examination on mechanically stimulated constructs confirmed the presence of the main constituents of cartilage ECM (Fig. 4C, only shown for the mechanical stimulated constructs). Safranin-O staining revealed a homogeneous deposition of GAGs after 28 days. Collagen type II deposition was mostly located around cells. Importantly, after mechanical conditioning both

MDZ and STMDZ constructs evidenced signs of gel mechanical failure, suggesting limited dynamic mechanical properties of the hydrogel. Pilot tests on non-reinforced hydrogels also revealed a similar type of hydrogel failure, however, at significantly lower compressive forces.

4 Discussion

The prime objective of this study was to engineer a regenerative implant that could capture the zonal mechanical properties of articular cartilage. In an attempt to mimic these properties, we have fabricated a composite construct that combined a bi-layered fibre scaffold with a hydrogel. To reproduce the superficial zone, we have printed a dense mat of crossed diagonal fibres. To reproduce the middle and deep zones, we have printed a box-like structure of multiple stacked fibres, as we previously demonstrated that it can synergistically improve the compressive properties of a GelMA hydrogel [12,13]. The fabrication of the entire bi-layered fibre construct was obtained with a single nozzle and in a single print, which is not possible by any other fibre formation process [8,21,22]. This provided us with the novel possibility of printing structurally-graded fibrous scaffolds in a continuous mode and allowed us to recreate a strong adhesion between STZ and the MDZ. However, it should be noted that this adhesion strength is dependent on the contact area and subsequent thermal bonding between the two layers. Moreover, despite the similarities between STMDZ architecture and native collagen structure, both inter collagen fibre spacing (100 nm) [23] and collagen fibre diameters (50-300 nm) [6] seen within native cartilage are significantly smaller than the printed ones (pore size ~50 μm at STZ and 800 μm at MDZ; fibre diameter ~20 μm), which is still a limitation of the MEW technology. Other research groups have also recently demonstrated the fabrication of meltelectrowritten multilayered fibre scaffolds for articular cartilage repair [24] and for culturing human adipose-derived stem cell (hASC) spheroids [25], however with simple uniform box-shaped microarchitecture with varying pore sizes through the scaffold thickness.

As hypothesized, the contribution of the STZ layer to the mechanical behavior of the composite constructs was more pronounced under incongruent type-loading. One explanation for this finding is that the inclusion of a thin superficial tangential zone reinforcing layer enabled the load to be distributed over a larger area recruiting a larger volume of the middle and deep reinforced region to carry compressive loads, and, therefore, more efficiently transfer the loads from directly loaded regions throughout all of the construct when the surface is compressed incongruently. Similar behavior has been observed in native articular cartilage [26–29]. Korhonen et al. demonstrated that the tangential collagen fibrils that occupy the STZ layer are fundamental to resisting compression induced by concentrated loads, such us indentation. In their study, compressive stiffness at both peak and equilibrium were higher for cartilage with a STZ layer than for STZ-deprived cartilage, and increased significantly with the STZ thickness [29]. Thambyah et al. and Bevil et al. have showed that the STZ not only ensures a uniform distribution of compressive loads applied locally but also stabilizes the collagen fibre network in the middle and deep zone [27,28].

Europe PMC Funders Author Manuscripts

In addition, our data also shows that both STZ and MDZ reinforced hydrogels have similar peak moduli under incongruent loading. This suggests that the STZ and MDZ fibre reinforcements enhance the hydrogel stiffness through two different mechanism. The MDZ reinforcement effect relates to the transferring of the indentation load into the reinforcing fibres oriented longitudinally. This results in the MDZ fibres being put under tension by the hydrogel lateral expansion. Also, another important reinforcement effect observed at the MDZ region is the resistance of the fibre cross-section interconnections to compressive loads. These interconnections are the result of multiple interlocked fibres that when combined with a hydrogel have a great capacity to carry compressive load, as previously demonstrated [13]. The STZ layer reinforcement effect is particularly important in the facilitating the hydrogel to carry load. That is, the placement of a thin STZ layer over a soft hydrogel allows the distribution of the locally applied compressive load sideways, and the reduction of the construct axial strain. Another less significant factor, is the resistance of the STZ fibres to tangential tensile forces generated during indentation at the hydrogel surface and the confinement of the hydrogel to lateral expansion inside of the STZ pores. Our findings on the effect of the STZ reinforcing also align well with previous observations by Hosseini et al. and others [26,30,31]. They demonstrated, based on the assumptions of a fibril-reinforced poroviscoleastic model of articular cartilage, that an intact superficial collagen network is fundamental for the load-sharing mechanism between directly loaded and adjacent cartilage. It is, however, important to mention that for the indentation loading, no direct comparisons between the determined mechanical characteristics, e.g. dependent on loading configuration and method, and existing literature can be performed since the actual contact conditions between the hemi-spherical ended indenter and the tested samples were not determined and therefore the material parameters, based on an assumed constitutive model, of the tested materials cannot be extracted. Future work will include extending an existing mathematical model [32] of fibre reinforced hydrogels in unconfined compression to examine their response to indenter loading, as well as the effect of the inclusion of an STZ layer.

Although the peak and equilibrium moduli of the STMDZ constructs did not match with the native cartilage, the trends in the ratio of the peak stress to equilibrium stress, as well as in the relaxation rates, were very similar to those for native cartilage. To the best of our knowledge, this is the first time that an engineered cartilage construct can capture the functional properties of both the STZ and MDZ zones of native cartilage. It is worth noting, however, that under congruent loading the peak modulus of cartilage increased upon removal of the STZ, in contrast to our engineered constructs. This increase can be explained by the rise in GAG content with the depth of the cartilage [33]. Under in-congruent loading, however, no significant differences in the cartilage peak modulus were observed upon STZ removal. This can be partly explained by the lower interstitial fluid pressurization inside of the cartilage as a result of the lower total deformation induced by the indentation loading. Furthermore, in the engineered STZ layer there is always contact between PCL fibres whereas in cartilage there are softer GAG rich regions between the collagen fibres which can also explain the differences between STDMZ and intact cartilage properties. Another difference between the natural cartilage and fibre-reinforced constructs was that the natural plugs were still attached to the underlying bone which would have substantially inhibited

radial expansion making them much stiffer. Important limitations of the current analysis are that the cartilage tissue was harvest from relatively young animals where the collagen architecture may not yet be fully developed and that cartilage thickness was greater than engineered constructs. Also, it is speculated that the effect of the engineered STZ layer will be more pronounced under dynamic loading conditions, since it is known that the native STZ plays a crucial role in facilitating the generation of high fluid load support during dynamic compression [33]. Such analysis on the dynamic compressive properties was not performed due to limitations with the hydrogel integrity after repeated compression.

Finally, we note that STMDZ reinforced hydrogels can support cartilaginous tissue formation upon physiologically relevant mechanical stimulation. When cultured under dynamic compression without TGF-ß1 supplementation, chondrocytes were able to produce GAGs and collagen type II in similar quantities to the STMDZ composites cultured in static conditions with TGF-ß1. However, no differences between the gels reinforced with the MDZ and the STMDZ architectures were observed. Two main inferences can be drawn from these results. First, the proposed mechanical conditioning protocol is capable of activating signalling factors that mediate neo-cartilage formation, without the need for continuous supply of exogenous TGF-ß1. This is one important step towards the clinical translation of these constructs, and is in line with previous findings by Stoddard et al. [34,35]. Secondly, that the differences in load distribution provided by the MDZ/STMDZ together with the dynamic indentation may not be sufficient to direct zonal cartilage ECM formation. From previous computational studies it is known that hemi-spherical shaped indenters can induce a mechanical condition that is closer to that observed in vivo and with that provide mechanical cues that could stimulate cells to produce a more physiological ECM structure [36,37]. A possible explanation for the results here reported is that gel fracturing was observed for the majority of the mechanical stimulated samples, which may have limited cell deformation and the subsequent activation of mechanotransduction cell signaling mechanisms, as described in the literature [38,39,40]. This is a potential limitation of this work suggesting the need for alternative hydrogels systems with improved fracture toughness. Also, to provide more in-depth read-outs regarding the zonal chondrocyte response to the engineered bi-layered constructs, future studies should consider to evaluate the expression of anabolic (e.g. aggrecan, collagen I & II & X) and catabolic (MMP13 and ADAMTS4) genes [41] at different STZ and MDZ regions. Ultimately, controlling the relaxation behavior of hydrogels by precisely engineering fibre reinforcing architectures opens up new possibilities to improve cartilage matrix formation in hydrogels. It was recently demonstrated that in fast relaxing hydrogels, with higher permeabilities, chondrocytes form wide regions of interconnected cartilage matrix [41]. Future studies are planned to quantify the permeability of the bi-layered reinforced hydrogels and explore how to best tune this physical property to enhance, and potentially drive, zonal neo cartilage formation.

5 Conclusion

In conclusion, we have demonstrated that it is possible to manufacture a well-defined and sophisticated bi-layered fibre structure that can approximate the functional properties of both the STZ and MDZ zones of native cartilage. The inclusion of a thin superficial tangential

Europe PMC Funders Author Manuscripts

zone reinforcing layer greatly improved the load-bearing properties the micro-fibre reinforced hydrogels, particularly under incongruent compressive loads. Our results also demonstrate that the new composite construct is able to support neo-cartilage formation upon physiologically relevant mechanical stimulation. However, further work is needed to improve dynamic mechanical properties of the gelMA hydrogel system. Taken together, we believe this is an important step towards the design of mechanically competent implants for cartilage regeneration.

Supplementary Material

Refer to Web version on PubMed Central for supplementary material.

Acknowledgements

The authors gratefully thank the strategic alliance University Medical Center Utrecht – Eindhoven University of Technology and the European Research Council (ERC) consolidator grant 3D-JOINT (#6474426) for their financial support. In addition, the authors are very grateful to Inge Dokter for all the support with the cell harvesting, in vitro culture and characterization; to Sylvia van Kogelenber and to Joost H van Duijn for their technical support with the fibre scaffold design and 3D printing process; and finally, to Jurgen Bulsink for the support with the bioreactor system design.

References

[1]. Wallace IJ, Worthington S, Felson DT, Jurmain RD, Wren KT, Maijanen H, Woods RJ, Lieberman DE. Knee osteoarthritis has doubled in prevalence since the mid-20th century. Proc Natl Acad Sci USA. 2017; 114(35):9332–9336. [PubMed: 28808025]

[2]. Chien Liao I, Moutos FT, Estes BT, Zhao X, Guilak F. Composite three-dimensional woven scaffolds with interpenetrating network hydrogels to create functional synthetic articular cartilage. Adv Funct Mater. 2013; 23(47):5833–5839. [PubMed: 24578679]

[3]. Mellati A, Fan CM, Tamayol A, Annabi N, Dai S, Bi J, Jin B, Xian C, Khademhosseini A, Zhang H. Microengineered 3D cell-laden thermoresponsive hydrogels for mimicking cell morphology and orientation in cartilage tissue engineering. Biotechnol Bioeng. 2017; 114(1):217–231. [PubMed: 27477393]

[4]. Levato R, Webb WR, Otto IA, Mensinga A, Zhang Y, van Rijen M, van Weeren R, Khan IlyasM, Malda J. The bio in the ink: cartilage regeneration with bioprintable hydrogels and articular cartilage-derived progenitor cells. Acta Biomater. 2017; 61:41–53. [PubMed: 28782725]

[5]. Fox AJS, Bedi A, Rodeo S. The basic science of articular cartilage: structure, composition, and function. Sports Health. 2009; 1(6):461–468. [PubMed: 23015907]

[6]. Camarero-Espinosa S, Rothen-Rutishauser B, Johan Foster E, Weder C. Articular cartilage: from formation to tissue engineering. Biomater Sci. 2016; 4:734. [PubMed: 26923076]

[7]. Glaser C, Putz R. Functional anatomy of articular cartilage under compressive loading quantitative aspects of global, local and zonal reactions of the collagenous network with respect to the surface integrity. Osteoarthr Cartil. 2002; 10(2):83–99. [PubMed: 11869068]

[8]. Chen H, de Botelho Ferreira A, van Braga Malheiro C, Blitterswijk C, Mota C, Wieringa PA, Moroni L. Direct writing electrospinning of scaffolds with multidimensional fiber architecture for hierarchical tissue engineering. ACS Appl Mater Interfaces. 2017; 9(44):38187–38200. [PubMed: 29043781]

[9]. Steele JAM, McCullen SD, Callanan A, Autefage H, Accardi MA, Dini D, Stevens MM. Combinatorial scaffold morphologies for zonal articular cartilage engineering. Acta Biomater. 2014; 10(5):2065–2075. [PubMed: 24370641]

[10]. Novak T, Seelbinder B, Twitchell CM, van Donkelaar CC, Voytik-Harbin SL, Neu CP. Mechanisms and microenvironment investigation of cellularized high density gradient collagen matrices via densification. Adv Funct Mater. 2016; 26:2617–2628. [PubMed: 27346992]

Europe PMC Funders Author Manuscripts

[11]. Ren X, Wang F, Chen C, Gong X, Yin L, Yang L. Engineering zonal cartilage through bioprinting collagen type II hydrogel constructs with biomimetic chondrocyte density gradient. BMC Musculoskelet. Disord. 2016; 17:301. [PubMed: 27439428]

[12]. Visser J, Melchels FPW, Jeon JE, van Bussel EM, Kimpton LS, Byrne HM, Dhert WJA, Dalton PD, Hutmacher DW, Malda J. Reinforcement of hydrogels using three-dimensionally printed microfibres. Nat Commun. 2016; 6:6933.

[13]. Castilho M, Hochleitner G, Wilson W, van Rietbergen B, Dalton PD, Groll J, Malda J, Ito K. Mechanical behavior of a soft hydrogel reinforced with three-dimensional printed microfibre scaffolds. Sci Rep. 2018; 8:1245. [PubMed: 29352189]

[14]. de Ruijter M, Ribeiro A, Dokter I, Castilho M, Malda J. Simultaneous micropatterning of fibrous meshes and bioinks for the fabrication of living tissue constructs. Adv Healthcare Mater. 2018

[15]. Guilak F, Ratcliffe A, Lane N, Rosenwasser MP, Mow VC. Mechanical and biochemical changes in the superficial zone of articular cartilage in canine experimental osteoarthritis. J Orthop Res. 1994; 12(4):474–484. [PubMed: 8064478]

[16]. Thibault M, Poole AR, Buschmann MD. Cyclic compression of cartilage/bone explants in vitro leads to physical weakening, mechanical breakdoan of collagen and release of matrix fragments. J Orthop Res. 2002; 20:1265–1273. [PubMed: 12472239]

[17]. Melchels FPW, Dhert WJA, Hutmacher DW, Malda J. Development and characterisation of a new bioink for additive tissue manufacturing. J Mater Chem B. 2014; 2:2282. [PubMed: 32261716]

[18]. Loessner D, Meinert C, Kaemmerer E, Martine LC, Yue K, Levett PA, Klein TJ, Melchels FPW, Khademhosseini A, Hutmacher DW. Functionalization preparation and use of cell-laden gelatin methacryloyl-based hydrogels as modular tissue culture platforms. Nat Protoc. 2016; 11(4):727–746. [PubMed: 26985572]

[19]. Thambyah A, Broom ND. Further insight into the depth-dependent microstructural response of cartilage to compression using a channel indentation technique. Comput Math Methods Med. 2013

[20]. Mouser VHM, Abbadessa A, Levato R, Hennink WE, Vermonden T, Gawlitta D, Malda J. Development of a thermosensitive HAMA-containing bio-ink for the fabrication of composite cartilage repair constructs. Biofabrication. 2017; 9

[21]. Fallahi A, Khademhosseini A, Tamayol A. Textile processes for engineering tissues with biomimetic architectures and properties. Trends Biotechnol. 2016; 34(9):683–685. [PubMed: 27499277]

[22]. Kang H, Zeng Y, Varghese S. Functionally graded multilayer scaffolds for in vivo osteochondral tissue engineering. Acta Biomater. 2018; 15(78):365–377.

[23]. DiDomenico CD, Lintz M, Bonassar LJ. Molecular transport in articular cartilage — what have we learned from the past 50 years? Nat Rev Rheumatol. 2018; 14:393–403. [PubMed: 29899547]

[24]. Bas O, Lucarotti S, Angella DD, Castro NJ, Meinert C, Wunner FM, Rank E, Vozzi G, Klein TJ, Catelas I, De-Juan-Pardo EM, et al. Rational design and fabrication of multiphasic soft network composites for tissue engineering articular cartilage: a numerical model-based approach. Chem Eng J. 2018:15–23.

[25]. Hrynevich A, Elçi BS, Haigh JN, McMaster R, Youssef A, Blum C, Blunk T, Hochleitner G, Groll J, Dalton PD. Dimension-based design of melt electrowritten scaffolds. Small. 2018; 14

[26]. Hosseini SM, Wu Y, Ito K, van Donkelaar CC. The importance of superficial collagen fibrils for the function of articular cartilage. Biomech Model Mechanobiol. 2014; 13:41–51. [PubMed: 23519459]

[27]. Thambyah A, Zhao J, Bevill SL, Broom ND. Macro-, micro- and ultrastructural investigation of how degeneration influences the response of cartilage to loading. J Mech Behav Biomed Mater. 2012; 5:206–215. [PubMed: 22100095]

[28]. Bevill SL, Thambyah A, Broom ND. New insights into the role of the superficial tangential zone in influencing the microstructural response of articular cartilage to compression. Osteoarthritis Cartilage. 2010; 18(10):1310–1318. [PubMed: 20633674]

[29]. Korhonen RK, Wong M, Arokoski J, Lindgren R, Helminen HJ, Hunziker EB, Jurvelin JS. Importance of the superficial tissue layer for the indentation stiffness of articular cartilage. Med Eng Phys. 2002; 24:99–108. [PubMed: 11886828]

[30]. Quiroga JMP, Wilson W, Ito K, van Donkelaar CC. Relative contribution of articular cartilage's constitutive components to load support depending on strain rate. Biomech Model Mechanobiol. 2017; 16:151–158. [PubMed: 27416853]

[31]. Sakai N, Hashimoto C, Yarimitsu S, Sawae Y, Komori M, Murakami T. A functional effect of the superficial mechanical properties of articular cartilage as a load bearing system in a sliding condition. Biosurface Biotribol. 2016; 2(1):26–39.

[32]. Chen, MJ, Kimpton, LS, Whiteley, JP, Castilho, M, Malda, J, Please, CP, Waters, SL, Byrne, HM. Multiscale modelling and homogenisation of fibre-reinforced hydrogels for tissue engineeringEur J Appl Math. Cambridge University Press; 2019. 1–29.

[33]. Gannon AR, Nagel T, Kelly DJ. The role of the superficial region in determining the dynamic properties of articular cartilage. Osteoarthritis Cartilage. 2012; 20(11):1417–1425. [PubMed: 22890186]

[34]. Li Z, Yao S, Alini M, Stoddart MJ. Chondrogenesis of human bone marrow mesenchymal stem cells in fibrin-polyurethane composites is modulated by frequency and amplitude of dynamic compression and shear stress. Tissue Eng A. 2010; 16(2):575–584.

[35]. Gardner OFW, Fahy N, Alini M, Stoddart MJ. Joint mimicking mechanical load activates TGFß1 in fibrin-poly(ester-urethane) scaffolds seeded with mesenchymal stem cells. J Tissue Eng Regen Med. 2017; 11:2663–2666. [PubMed: 27445107]

[36]. Khoshgoftar M, van Donkelaar CC, Ito K. Mechanical stimulation to stimulate formation of a physiological collagen architecture. Comput Methods Biomech Biomed Eng. 2011; 14:135–144.

[37]. Lee EJ, Holmes JW, Costa KD. Remodeling of engineered tissue anisotropy in response to altered loading conditions. Ann Biomed Eng. 2008; 36:1322–1334. [PubMed: 18470621]

[38]. Mauck RL, Wang CC, Oswald ES, Ateshian GA, Hung CT. The role of cell seeding density and nutrient supply for articular cartilage tissue engineering with deformational loading. Osteoarthritis Cartilage. 2003; 11(12):879–890. [PubMed: 14629964]

[39]. Cochis A, Grad S, Stoddart MJ, Farè S, Altomare L, Azzimonti B, Alini M, Rimondini L. Bioreactor mechanically guided 3D mesenchymal stem cell chondrogenesis using a biocompatible novel thermo-reversible methylcellulose-based hydrogel. Sci Rep. 2017; 23(7)

[40]. Steinmetz NJ, Aisenbrey EA, Westbrook KK, Qi HJ, Bryant SJ. Mechanical loading regulates human MSC differentiation in a multi-layer hydrogel for osteochondral tissue engineering. Acta Biomater. 2015; 21:142–153. [PubMed: 25900444]

[41]. Lee H, Gu L, Mooney DJ, Levenston ME, Chaudhuri O. Mechanical confinement regulates cartilage matrix formation by chondrocytes. Nat Mater. 2017:16. [PubMed: 29180779]

Europe PMC Funders Author Manuscripts

Europe PMC Funders Author Manuscripts

Statement of Significance

Damage to articular cartilage results in severe pain and joint disfunction that cannot be treated with currently available implants. This study presents a sophisticated bioengineered bi-layered fibre reinforced cell-laden hydrogel that can approximate the functional mechanical properties of native cartilage. For the first time, the importance of incorporating a viable superficial tangential zone (STZ) - like structure to improve the load-bearing properties of bioengineered constructs, particularly when in-congruent surfaces are compressed, is demonstrated. The present work also provides new insights for the development of implants that are able to promote and guide new cartilaginous tissue formation upon physiologically relevant mechanical stimulation.

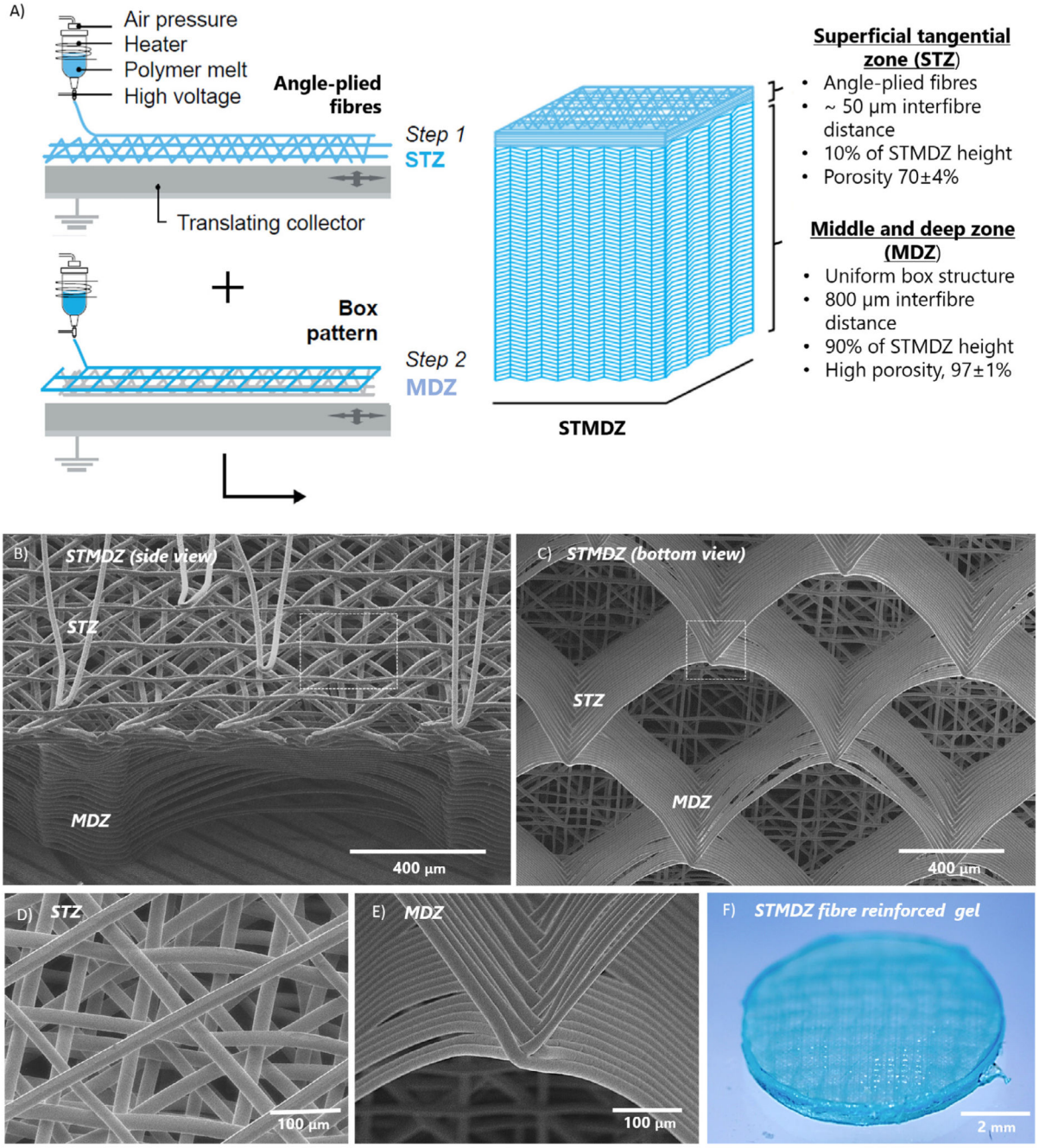

Fig. 1.

Design and 3D printing of fibre reinforced hydrogels with a superficial tangential zone. A) Design approach and sequential melt electrowriting of the bi-layered fibre scaffolds. SEM images of printed STMDZ fibre constructs from B) side view and C) bottom view. Detail of D) angle-ply fibre deposition at STZ and E) accurately stacked fibres at MDZ. F) Stereoscopic image of a representative GelMA gel reinforced with the STMDZ microfibre scaffold.

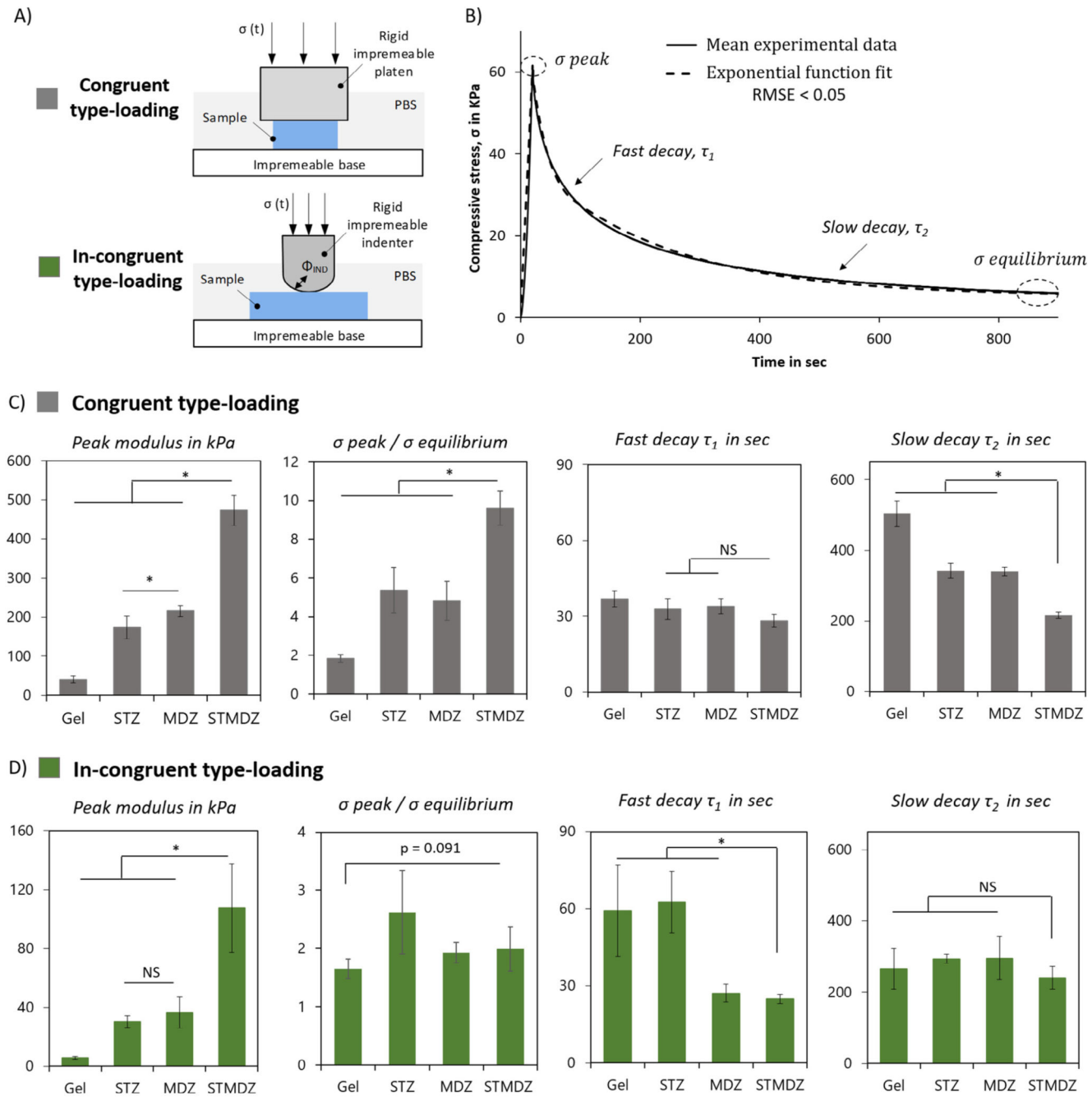

Fig. 2.

Effect of superficial tangential zone on engineered hydrogel-fibre composites mechanical behavior. A) Schematics of the loading methodologies used: unconfined compression geometry (congruent type-loading), and indentation methodology (in-congruent type-loading). B) Representative stress relaxation curve of tested constructs, showing the fast and slow relaxation phase, and corresponding exponential model fit (RMSE < 0.05) with determined mechanical parameters. C) Comparison of time-dependent mechanical properties: apparent peak modulus, peak stress: equilibrium stress ratio, and time constants,

Europe PMC Funders Author Manuscripts

short decay (τ_1) and long decay (τ_2) for C) congruent-type loading and D) incongruent-type loading of gel alone, superficial tangential zone (STZ), middle and deep zone (MDZ), and superficial tangential and middle and deep zone reinforced constructs (STMDZ). *Indicates a significant difference, p = 0.05, and NS indicates non-significant difference.

Europe PMC Funders Author Manuscripts

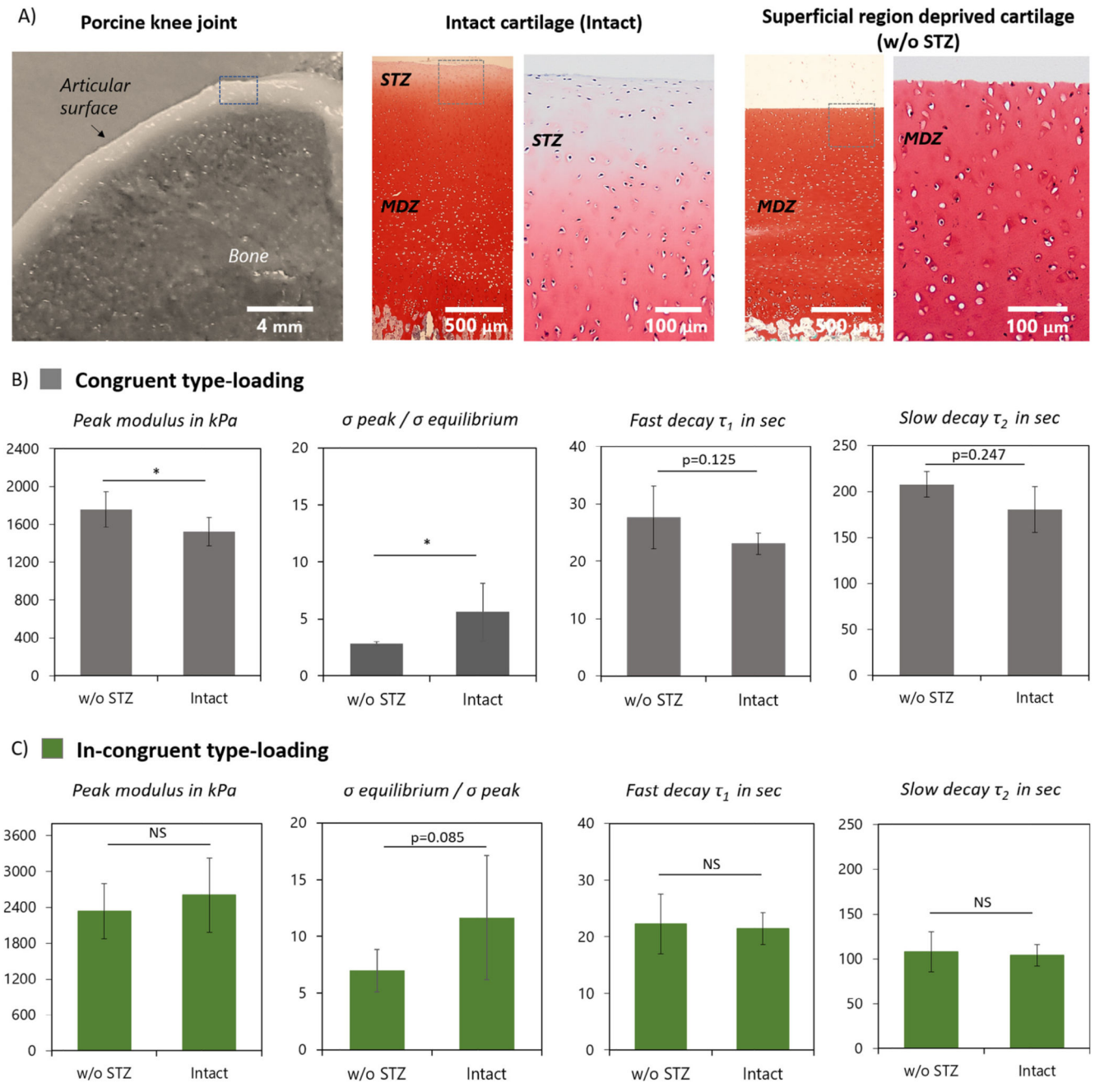

Fig. 3.

Effect of superficial tangential zone on articular cartilage mechanical behavior A) Osteochondral plugs isolated from porcine knee joints before (intact) and after superficial tangential zone removal (w/o STZ). Safranin-O stain displays an increase in GAG content with cartilage depth. Comparison of time-dependent mechanical properties of intact and w/o STZ cartilage samples under B) congruent and C) in-congruent type loading. *Indicates a significant difference, p = 0.05, and NS indicates nonsignificant difference, p > 0.25. p values within 0.05 and 0.25 are also considered significant and specific values are indicated.

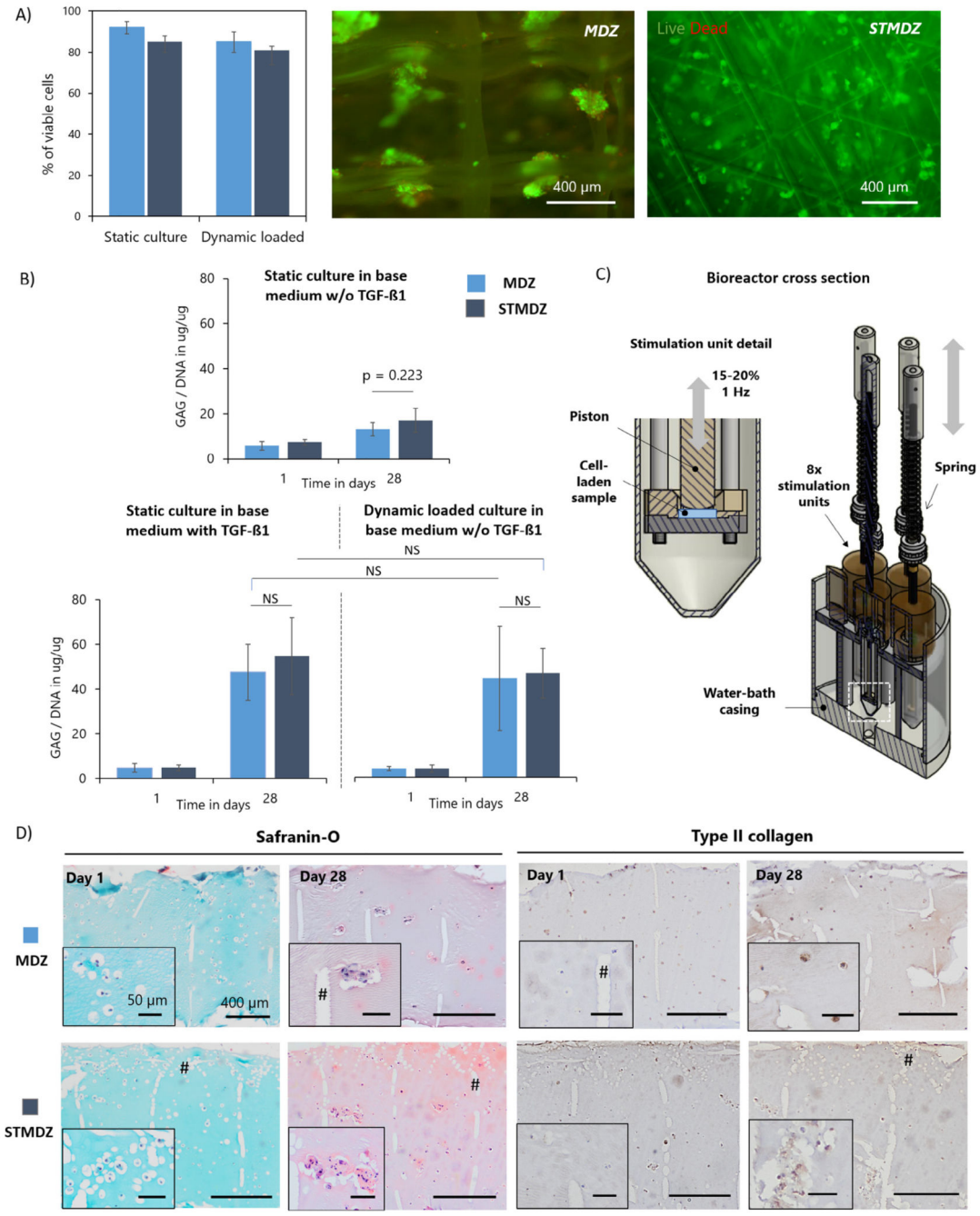

Fig. 4.

Neo-cartilage formation in gelMA hydrogel reinforced constructs. A) Cell viability and distribution in MDZ and STMDZ hydrogel composites at day 1 of static and dynamic loading conditioning in base medium w/o TGF-ß1. Viable cells are stained in green and dead cells in red. B) GAG content normalized to DNA of the static and dynamically loaded constructs at day 1 and 28. C) Schematic representation of the dynamic compression bioreactor. Cross section of the single station bioreactor system and stimulation units. D) Histological analysis of dynamic loaded constructs at day 1 and 28. Some MEW fibres are

Europe PMC Funders Author Manuscripts

indicated with #. Scale bars represent 400 μm and 50 μm. NS indicates non-significant difference. (For interpretation of the references to colour in this figure legend, the reader is referred to the web version of this article.)

Europe PMC Funders Author Manuscripts